

Short-term variability and summer-2009 averages of the mean wind and tides in the mesosphere and lower thermosphere over Langfang, China (39.4°N, 116.7°E)

Cunying Xiao^{a,*}, Xiong Hu^a, Anne K. Smith^b, Qingchen Xu^a, Xuxing Chen^{a,c}

^a Center for Space Science and Applied Research, CAS, Beijing 100080, China

^b Atmospheric Chemistry Division, National Center for Atmospheric Research, Boulder, Colorado, USA

^c Graduate University of Chinese Academy of Sciences, Beijing 100080, China

ARTICLE INFO

Article history:

Received 25 April 2012

Received in revised form

30 July 2012

Accepted 9 October 2012

Available online 7 November 2012

Keywords:

MF radar

Mean wind

Atmospheric tide

Mesosphere and lower thermosphere (MLT)

HWM model

GSWM model

ABSTRACT

Data obtained from the newly installed MF radar at Langfang (39.4°N, 116.7°E), China, during the summer months of 2009 are used to study the short-term variability and summer averages of the mean wind and tidal oscillations in the mesosphere and lower thermosphere (MLT). Both the zonal and meridional daily winds between 80 km and 98 km show considerable day-to-day variability; their Lomb–Scargle spectra reveal active quasi-2-day and quasi-16-day planetary waves. The tidal large day-to-day variations have time scales of days or longer, which could be attributed to the contribution of planetary waves. The summer-averaged zonal wind is westward below 82 km and eastward above 88 km with the transition altitude at ~85 km. The meridional wind is dominated by the southward wind. The summer-averaged zonal and meridional semidiurnal tides exhibit amplitudes of 10–15 m/s; they are larger than the diurnal tides, whose amplitudes are 5–10 m/s. The phase tilt of the semidiurnal tide is downward, indicating this component is excited below the MLT. For the diurnal tide, the phase propagation is downward above 86 km but it is upward below 86 km, which indicates that the tide is evanescent or a mixture of evanescent and propagating modes. These wind and tide observations are compared with data from other mid-latitude stations at ~40°N and with the HWM and GSWM models. Comparisons show that HWM-93 is better than HWM-07 in delineating the 2009 summer-averaged zonal wind over Langfang while both have systematic discrepancy in delineating the meridional mean winds. The prediction of the 2009 summer-averaged diurnal tide over Langfang by GSWM-09 is better than that from GSWM-02 but not the semidiurnal tide.

© 2012 Elsevier Ltd. All rights reserved.

1. Introduction

In recent decades dynamics of the mesosphere and lower thermosphere (MLT) has attracted great interest and has been the subject of many experimental and theoretical investigations. Atmospheric solar tides with periods of one day or its subharmonics are among the most important components of the dynamics and are known to play an important role in the energy and momentum budget of the MLT (Groves and Forbes, 1985; Forbes et al., 1993). The tides also modulate the flux of propagating gravity waves (Manson et al., 1998) and have significant impacts on the distributions of atmospheric constituents (Shepherd et al., 1998).

Tidal structures in MLT are extremely complex. There have been many investigations of their characteristics that have taken

advantage of rapid improvements in the quantity and quality of observational data, primarily from radar, lidar and satellite observations (e.g., Yuan et al., 2008; Pancheva et al., 2009; Lu et al., 2011). Previous observations have shown that the diurnal and semidiurnal components are the largest tidal modes in the MLT and that their features vary with latitude (e.g., Manson et al., 2002). At low latitudes, the primary mode is the diurnal tide while at latitudes greater than ~40°N/S the semidiurnal tide dominates. Manson et al. (2003) compared medium frequency (MF) radar observations of tides at Platteville (40°N, 105°W) and Saskatoon (52°N, 107°W). They found that the 24-hour tide dominates at 40°N and the 12-hour tide dominates at 52°N. Moreover, with data from the CUJO (Canada U.S. Japan Opportunity) radar (MF) network (sites 40–45°N), Manson et al. (2004a) demonstrated that the longitudinal variability of the tides is significant. Longitudinal differences in the semidiurnal tide were also found by Friedman et al. (2009) in the low-latitude mesopause region (83–103 km) using observations from two sites: Arecibo, Puerto Rico (18.3°N, 66.8°W) and Maui, Hawaii (20.7°N,

* Correspondence to: No.1 Nanertiao, Zhongguancun, Haidian district, Beijing 100190, China. Tel.: +86 10 62555987; fax: +86 10 62565649.

E-mail address: xiaocy@nssc.ac.cn (C. Xiao).

156.3°W). Satellite observations of daytime and nighttime winds between $\pm 40^\circ$ latitude at 95 km from the High Resolution Doppler Imager (HRDI) and Wind Imaging Interferometer (WINDII) on the Upper Atmospheric Research Satellite (UARS) showed significant longitudinal variations in tidal structure (Forbes et al., 2003). New observations near 40°N but at a different longitude than previously observed are valuable because they provide additional information for a latitude range where both the diurnal and semidiurnal tides are important. In particular, they can be used for investigating the longitudinal structure of the tides.

Since June 2009, a new MF radar has been in continuous operation at Langfang, China (39.4°N , 116.7°E), providing zonal and meridional wind measurements. In the present paper, the wind data from June 4 to August 31, 2009, obtained from this MF radar are used to study the characteristics of short-term variations and summer-averages of winds, diurnal and semidiurnal tides. These observations will be compared and contrasted with those reported by other stations, especially the MF results at Urbana (40°N , 88°W) (Franke and Thorsen, 1993), Platteville (40°N , 105°W) (Manson et al., 2003), Fort Collins (41°N , 105°W) (She et al., 2004; Yuan et al., 2008), all of which are located near 40°N . The summer averages will also be compared with the latest versions of the well-used HWM (Horizontal Wind Model) and GSWM (Global Scale Wave Model).

The motive of this work is to report the characteristics of prevailing winds and atmospheric tides over Langfang during summer-2009, enriching the winds and tidal observations at $\sim 40^\circ\text{N}$. Considering the facts that HWM-93 and GSWM-02 are the most popular versions of neutral wind and tidal models, respectively, and are often involved in the past and still current papers, while the HWM-07 and GSWM-09 are the newest versions and may be used widely in the near future, it makes sense in comparing the observations with these two versions of the HWM and GSWM models at the present stage. In this paper, we will compare the observations of mean winds with the HWM-93 and HWM-07, and compare the observations of tides with GSWM-02 and GSWM-09 to determine the differences of the two different versions in delineating the real atmosphere over Langfang. Although the analysis is focused on only 3 months data, this work can provide valuable references to the improvement of the models.

Section 2 provides an overview of the radar system and data collection and analysis methods. Section 3 describes the HWM and GSWM models. Section 4 shows the results and discusses the short-term variations and summer averages of the measured horizontal winds and their comparison with other stations and with HWM. Section 5 presents and discusses the measurements of tides and comparisons with GSWM predictions. Finally, Section 6 gives the conclusions.

2. Langfang MF radar system and data analysis methods

A new MF radar which uses the spaced-antenna technique was established at Langfang, China (39.4°N , 116.7°E), in May 2009. The MF radar operates at a frequency of 1.99 MHz and employs four sets of crossed dipoles for transmitting and receiving. The four antenna sub-arrays are arranged in a ‘Y’ pattern with a spacing of 181 m. Table 1 gives the specifications of the radar system. Since June 4, 2009, the radar has been used to measure winds and electron densities in the 60–100 km height range. Electron densities and vertical winds will not be discussed in this paper. Wind measurements are made at 2 km height intervals and at time intervals of 4 min; the actual measurement schedule is 2 min for winds alternating with 2 min for electron densities.

Table 1
Langfang MF radar system specifications.

Characteristic	
Location	39.4°N , 116.7°E
Operating frequency	1.99 MHz
Peak envelope power	64 kW
Half-power pulse width	22.8 μs
Antenna spacing	181 m
Pulse repetition frequency	80 Hz (day)/40 Hz (night)
Coherent integration	32(day)/16(night)
Sampling interval	2 km
Time resolution	4 min
Height range	60–100 km

The complex auto- and cross-correlations functions obtained with 260-point time series are parameterized in real-time to obtain true velocity estimates using the commonly used and accepted full correlation analysis algorithm (e.g., Briggs, 1984).

Using 3-month quasi-continuous observations from June 4 to August 31 2009, with gaps from June 18 to 19 and from August 22 to 25, studies of the prevailing winds and atmospheric tides have been made. Fig. 1 indicates the average number of wind estimates available per hour at each height gate (between 60 and 100 km) during the summer months (June, July, and August) at Langfang. It should be noted that all of the data presented in this study are plotted in terms of virtual height. Namboothiri et al. (1993) studied the effects of group retardation on 2.2-MHz received echoes at Saskatoon. They showed that, in summer daytime, the virtual height is approximately equivalent to the real height up to 97 km during solar minimum periods and up to 95 km during solar maximum. Similar constraints are applicable to the Langfang results in June–August 2009, which is during solar minimum. We caution that results at 97 km and above may be biased by the effects of group retardation. Fig. 1 shows that the distribution of data rates in the three months are quite similar to each other. In all months, there are diurnal variations in data yield. The average number of wind estimates is low at 60–68 km during daytime and at 60–80 km during nighttime. Generally, the daytime is characterized by a larger number of wind estimates than the nighttime. The maximum data rate is observed near 80–90 km at ~ 4 UT (12 LT). Wind data used in the present study cover the altitude region 80–98 km where nearly continuous 24-hour coverage is available.

The hourly averaged mean winds (centered about the half hour) at each height of observation from 80 km to 98 km are used in the analysis procedure. Classical harmonic analysis is performed to retrieve the mean wind and tidal components. For this, the hourly mean data are divided into 24 h blocks and then subjected to least-squares fit with a constant, 24 h, 12 h and 8 h components. When there are short gaps in the data, these are simply omitted from the least squares fitting routine without seriously affecting the results. Fits are accepted with a minimum of 16 h of data. Moreover, fits are rejected if the root mean square errors (RMSE) produced by the fitting procedure are unacceptably large; here the cutoff is 2 times the mean RMSE in summer at each height. Thus it is believed that any data that might bias the conclusions have been rejected.

The mean wind is obtained from the constant component of the harmonic analysis of the daily data. Thus the short-term variability, such as day-to-day changes in the mean wind and tides, can be captured. Moreover, the daily zonal and meridional mean winds and the 24 h, 12 h and 8 h components are used to form the seasonal means.

The zonal and meridional components are calculated as follows. Firstly, for each height and 24 h time interval, the means

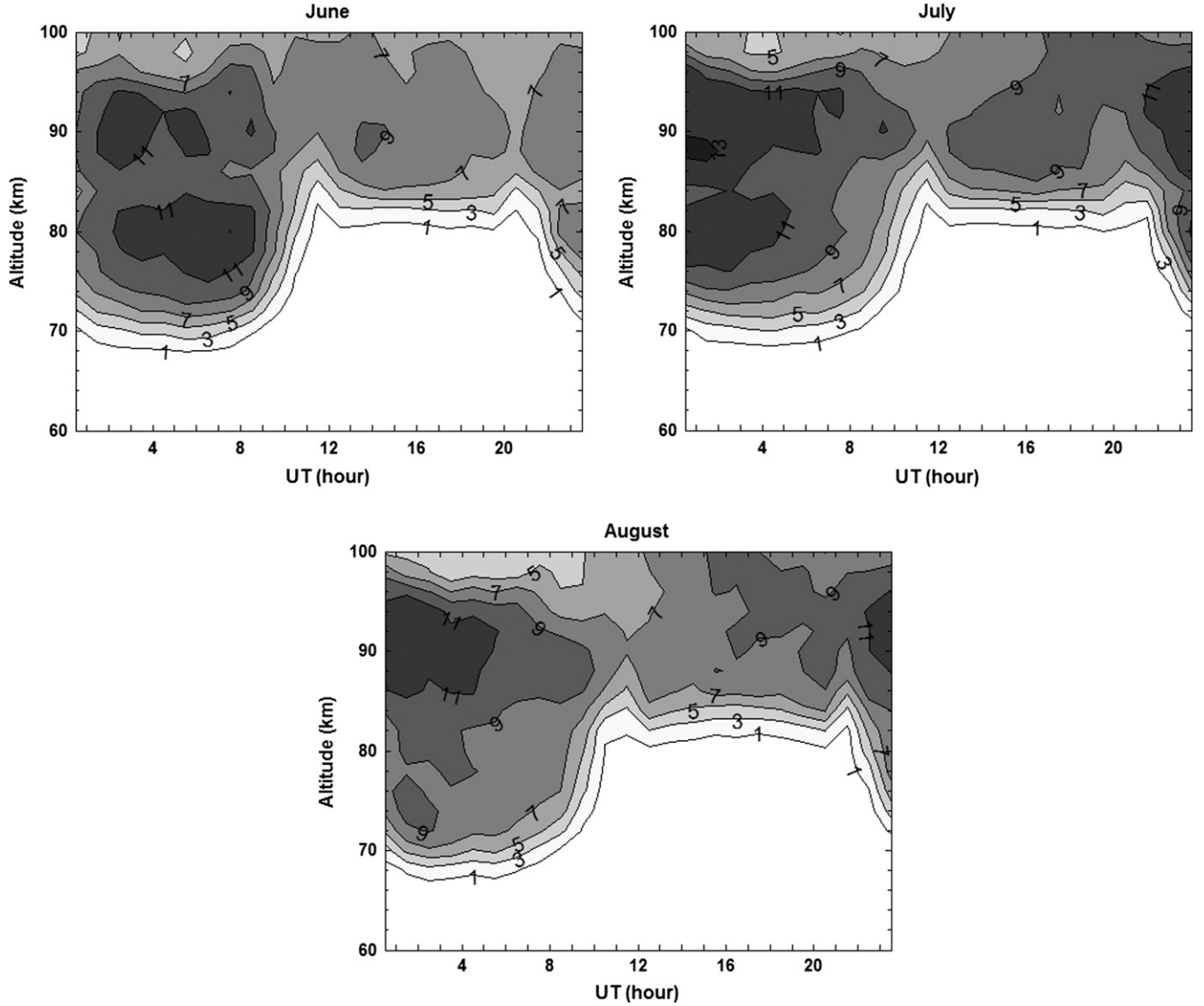


Fig. 1. Average number of wind estimates available per hour at each height gate (between 60 and 100 km) in June, July, and August 2009 at Langfang. Maximum number possible is 15 estimates/h. Local time (LT) is universal time (UT) plus 7.78 h.

and 24 h, 12 h and 8 h components are used to reconstruct the winds at fixed hours t_i by

$$U_i(t_i) = U_0 + U_{24\text{h}} \cos\left(\frac{2\pi}{24}(t_i - \phi_{24\text{h}})\right) + U_{12\text{h}} \cos\left(\frac{2\pi}{12}(t_i - \phi_{12\text{h}})\right) + U_{8\text{h}} \cos\left(\frac{2\pi}{8}(t_i - \phi_{8\text{h}})\right) \quad (1)$$

Here, U is the zonal or meridional component; U_0 is the daily mean; $U_{24\text{h}}$, $U_{12\text{h}}$, $U_{8\text{h}}$ and $\phi_{24\text{h}}$, $\phi_{12\text{h}}$, $\phi_{8\text{h}}$ are the amplitudes and phases of the 24 h, 12 h and 8 h components, respectively. t denotes the time in hour, that is, $t_i = (i-0.5)\text{h}$, $i=1, 2, 3 \dots 24$. Secondly, at each observation height and hour t_i , all the available U_i during the summer season are averaged to get the seasonal mean \bar{U}_i , $i=1, 2, 3 \dots 24$. Thirdly, the least squares fitting is applied to the seasonal averaged \bar{U}_i to determine the seasonal averaged zonal and meridional winds and the amplitudes and phases of the tides. Fourthly, for the zonal and meridional winds, diurnal and semidiurnal tide's amplitudes and phases, root mean square differences (RMSD) between the available daily and seasonal averages are calculated respectively.

The number of days with available observations based on our criterions is 18 days at 80 km, 56 days at 82 km, 66 days at 84 km, and 73 days between 86 km and 98 km. Readers may be concerned about whether the difference in days of averaging affects the results, especially in discussion of the mean tidal phase tilts and their vertical wavelengths. We have tested just by using 56-day averaging as at 82 km and 66-day averaging as at 84 km. Results show that the difference in days of averaging does not affect the structure and tilt of the seasonal averaged curves. Thus, we will use all the available days in the summer averages. However, as the much lower number of available days at 80 km, the main discussions are focused on the altitude range of 82–98 km; the mean values in the figures in this paper at 80 km can be treated as a reference.

Throughout the analysis and discussion of the results the following conventions are used to describe the wind and tide components. Positive wind amplitude refers to a wind directed towards the east or north (eastward or northward) for zonal and meridional components, respectively. The phase of the zonal tidal components is defined as the local time (LT) in hours at which the maximum eastward wind velocity occurs, and the phase of the

meridional tidal components is defined as the LT of maximum northward wind velocity.

3. HWM and GSWM models

3.1. HWM models

The HWM is an empirical model of the horizontal neutral wind. The first edition of the model released in 1987 (HWM-87) was intended for winds above 220 km (Hedin et al., 1988). With the inclusion of wind data from ground-based incoherent scatter radar and Fabry–Perot optical interferometers, HWM-90 (Hedin et al., 1991) was extended down to 100 km and using MF/Meteor data HWM-93 (Hedin et al., 1996) was extended down to the ground. HWM-93 provides a single analytic model for calculating zonal and meridional wind profiles representative of the climatological average for various geophysical conditions. For a number of years, MF/meteor radar data have been compared with HWM-93 to assess the quality of the radar systems. Results showed satisfactory agreement for the mean zonal winds but some discrepancy for the meridional winds (e.g., Xiao et al., 2007; Buriti et al., 2008; Andrioli et al., 2009).

In the development of HWM-07, Drob et al. (2008) and Emmert et al. (2008) overhauled the model parameterization and added a significant number of new data to the HWM-93 model. HWM-07 consists of two parts: a quiet-time portion, and a geomagnetically disturbed portion. In addition to the data used in HWM-93, HWM-07 is based on extensive new ground-based and space-based wind measurements, including height profiles from NASA-UARS/WINDII, NASA-UARS/HRDI, measurements from ground-based optical and radar instruments obtained from the NSF-CEDAR database, and

lower atmospheric NCEP data. Thus, we could expect that the ability of HWM07 to represent the available observational data and the true behavior of the atmosphere is better than that of HWM-93. In the present work, the prevailing winds over Langfang observed with its MF radar will be compared with HWM-07 and also with HWM-93 to determine the differences of the two versions in delineating the atmosphere in 2009 summer over Langfang.

3.2. GSWM models

The GSWM is a numerical model of planetary waves and solar tides in the earth's atmosphere from the ground to the thermosphere developed at HAO (High Altitude Observatory), NCAR. GSWM solves for non-migrating and migrating waves with two-dimensional, linearized, steady-state assumptions. The GSWM model has undergone several versions. GSWM-02 is the most popular version since its publication in 2002 (Hagan and Forbes, 2002). It incorporates the radiational tides resulting from non-longitudinally varying forcing and the tides (non-migrating as well as the migrating), forced by tropospheric latent heat processes, include the “standing” (wave number 0) diurnal and semi-diurnal tidal oscillations along with eastward and westward propagating harmonics with wave-numbers 1–6 (Hagan and Forbes, 2002; 2003).

The comparisons of MLT tides observed by MF/meteor radar or by satellites with GSWM models show encouraging similarities and also significant differences. For example, Manson et al. (2002) compared semi-diurnal and diurnal tides from MF radar observations from 2–70°N with the GSWM-00 model and found significant differences. Jiang et al. (2010) compared the Fuke meteor radar observations to GSWM-02 and reported that the diurnal tide agreed well with the model but many differences were found

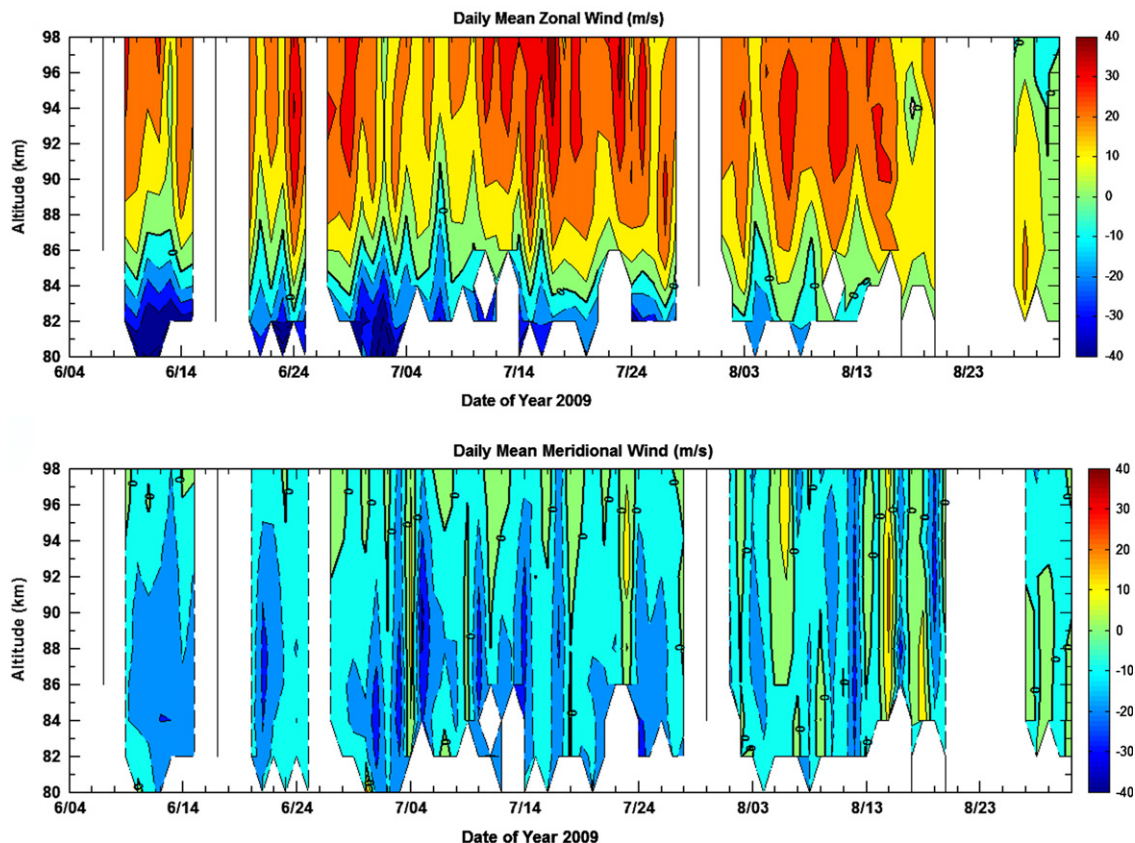


Fig. 2. Temporal variations of the daily mean zonal and meridional winds at heights from 80 km to 98 km. (Contour intervals are 10 m/s, with the solid lines denoting eastward or northward winds, dashed lines the opposite directions, and the thick black lines the zero wind line.)

for the semidiurnal tide. Manson et al. (2004b) compared the diurnal and semidiurnal tides observed from HRDI/UARS with GSWM-02 results; they reported that the model 24-h tidal amplitudes are larger than observed during the equinox poleward of 40° latitude while the model 12-h tidal amplitudes are much smaller than observed during non-winter months poleward of 30° .

Recently, Zhang et al. (2010a, b) reported updated GSWM-09 nonmigrating tidal climatologies in which the model is driven using the updated latent and radiative heating rates based upon International Satellite Cloud Climatology Project (ISCCP) and Tropical Rainfall Measuring Mission (TRMM) observations. Iimura et al. (2011) showed the Arctic and the Antarctic tides measured by MF radars compared to the GSWM-09. Herein, we present the signatures of diurnal and semidiurnal tides observed by the Langfang MF radar and compare these tides with GSWM-09 and also with GSWM-02 to investigate whether the updates in GSWM-09 affect the simulation of the observed characteristics of these tides in the MLT region in 2009 summer over Langfang.

4. Results and discussions: mean winds

This section presents the temporal and height variations of horizontal mean winds at the heights between 80 and 98 km and the comparisons with the HWM-93 and HWM-07 empirical wind models.

4.1. Short-term variation of the mean winds

Fig. 2 shows the temporal and height variations of the daily mean horizontal winds. Results exhibit considerable short-term variations in both zonal and meridional daily mean winds. The daily mean zonal wind varies from -40 m/s to 40 m/s (positive eastward) and is always westward below 82 km and eastward above 88 km; the transition from westward to eastward occurs at about 85 km. The meridional daily mean wind varies from -35 m/s to 20 m/s (positive northward). Generally, the wind is southward during the whole observational period except on 4 July, 17 and 20 August. The strength of the southward wind increases with increasing height and then decreases; the largest value of -35 m/s is at about 90 km on 5 July. Similar large short-term variations in the wind field had also been reported at other sites, for example, at Wuhan (30°N , 114°E) by the MF radar (Zhang et al., 2004) and at Andoya/Norway (69°N , 16°E) by the mobile SOUSY VHF radar (Yi, 2001).

In addition, for both zonal and meridional winds, the day-to-day variations are very pronounced with time scales on the order of days or longer. Large-scale variations are often superposed with smaller-scale fluctuations. In order to show the spectral breakdown of the variability, spectral analysis is used to the daily mean winds. At a fixed height, there are time series data for both the zonal and meridional daily mean winds, which are the input signals. Lomb–Scargle periodogram method (Press et al., 1992) is applied with the sliding window of length of 48 days, which is marked with the middle day. The window is shifted by 1 day, and the number of the data should be no less than 32. The Lomb–Scargle spectra are oversampled with a factor of 16; the spectral estimate is then calculated at the frequency interval $1/(48 \times 16)$ between $1/48$ and $1/2$.

As a typical example, Fig. 3 shows the dynamic power spectrum of the zonal daily mean wind at the height of 90 km. The x-axis is the frequency of the wind fluctuation and the y-axis is the time axis. The color bar indicates the normalized power. Inside of the color bar and the figure, the confidence levels of 90% and 50% are shown. The spectrum is dominated the whole time by

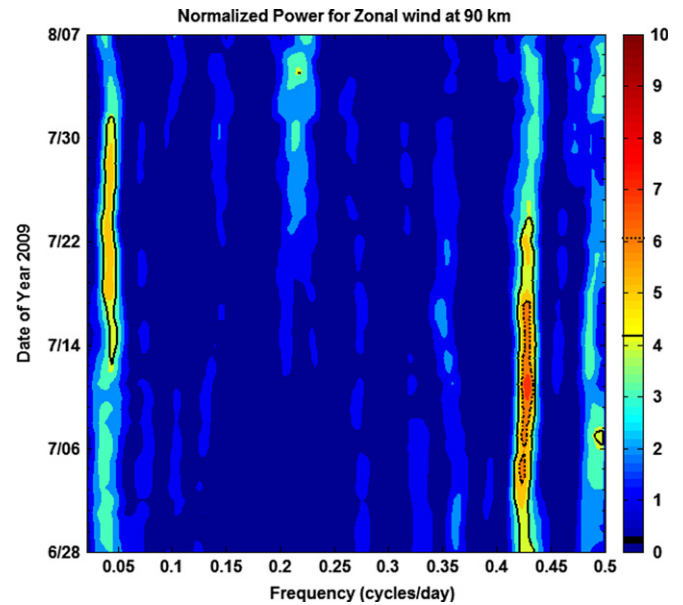


Fig. 3. Dynamic power spectrum of the zonal daily mean wind at the height of 90 km. On the x-axis is the frequency of the wind fluctuation and on the y-axis the time. The times on the y-axis represent the middle of a 38-day data window. The confidence levels (90%, 50%) are drawn with solid lines and dot lines.

the frequencies of 0.043 cycles/day and 0.43 cycles/day, which denote the 23-day and 2.3-day waves, respectively. The 2.3-day wave is prominent on the dates from 3 July to 17 July with confidence larger than 50%, especially on 11 July with the confidence of about 98%. The 23-day wave is found larger confidence than 50% from 13 July to 1 August. Moreover, waves at 0.22, 0.35 and 0.495 cycles/day are also visible, corresponding to the periods of 4.5-day, 2.9-day, and 2-day, respectively.

4.2. Summer-averaged winds

The summer-averaged zonal and meridional winds observed by the Langfang MF radar are shown in Fig. 4. The horizontal bars in the figure indicate the RMSD from the daily mean winds to the summer averages, which represent the day-to-day variability of the mean winds. The summer-averaged zonal wind is westward below 84 km. Above 86 km, the wind is eastward and the speed increases with the height to a maximum of ~ 22 m/s at about 94 km, then decreases above there. The reversal height of the summer zonal wind is at about 85 km, which is quite similar to that seen at Urbana (40°N , 88°W) (Franke and Thorsen, 1993) but about 5 km higher than that over Yamagawa (31.2°N , 130.6°E) (Xiao et al., 2007) and about 5 km lower than that over Poker Flat, Alaska (65.1°N , 147.5°W) (Kishore et al., 2002). The RMSD of zonal winds are always within 10 m/s.

The summer-averaged meridional wind is southward. The maximum value is about 8 m/s at the height of 82–86 km and the lowest value is 2–3 m/s at 98 km. This mean wind structure has general similarities to those measured by the Yamagawa (31.2°N , 130.6°E) MF radar (Xiao et al., 2007), which is located about 8 degree further south and 14 degrees to the east. However, the meridional wind at Urbana (40°N , 88°W), which is at almost the same latitude as Langfang but 155 degrees apart in longitude, was dominated by the northward wind above 85 km in summer (Franke and Thorsen, 1993). The RMSD of meridional wind are about 10 m/s and do not vary much with height.

Also shown in Fig. 4 are the summer-averaged (June, July and August) winds obtained from the HWM-93 and HWM-07 models with the purpose of presenting comparisons between the MF

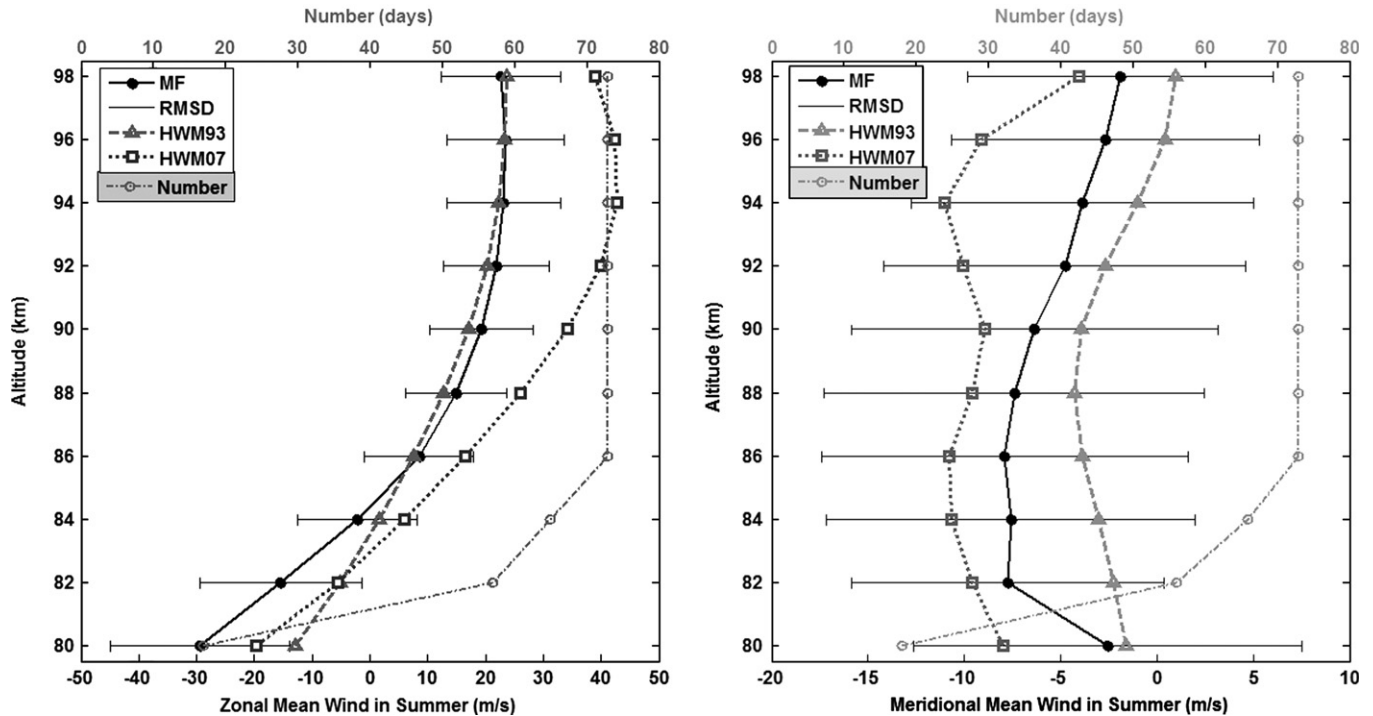


Fig. 4. Summer-averaged profiles of zonal and meridional winds. The solid lines with filled circles denote the results of MF radar, the dashed lines with upward-pointing triangles and the dotted lines with squares indicate the HWM-93 and HWM-07 model results, respectively. The solid horizontal bars denote the RMSD from the daily mean winds to the summer averages. The Dash-dot lines with circles give the number of days with observations.

observations and the models. For the zonal direction, all the profiles are similar. HWM-93 and HWM-07 underestimate the height of the summer reversal seen at Langfang by about 1 km and 1.5 km, respectively. The zonal mean wind derived from HWM-07 is about 10–20 m/s larger than the MF observation with the maximum difference at about 94 km. The HWM-93 zonal wind is quite similar to the observation above 84 km, but is lower than the observed zonal mean wind below 82 km. The differences between HWM-93 and the MF zonal mean winds are within the RMSD from the daily mean zonal winds to the summer averages while the HWM-07 results are outside the RMSD above 88 km.

For the meridional mean winds, systematic discrepancies are found between the MF observation and both HWM-93 and HWM-07. In HWM-07, the summer-averaged meridional wind is southward from 80 to 98 km; the model overestimates the MF wind values by 2–7 m/s. The summer-averaged meridional wind obtained from HWM-93 is northward above 96 km and southward below and the speeds are lower than the observations at all levels. The HWM-93 meridional wind is 1–6 m/s weaker than the MF observed profile with the largest difference of 6 m/s at 82 km. The vertical gradients are different among the three profiles. The observed meridional mean wind increases with the increasing height, reaching the maxima at 82–86 km, and then decreases with height. The HWM-93 meridional mean wind also increases and then decreases with the increasing height, but with the maximum wind value at 88 km. Two maxima, located at 86 km and 94 km, are found in the HWM-07 meridional mean wind profile. All the differences between the models and the MF observations are within the RMSD from the daily mean meridional winds to the summer averages.

Based on these detailed comparisons of both the zonal and meridional mean winds, we can come to the conclusion that the HWM-93 is better than HWM-07 in delineating the 2009 summer-averaged zonal wind over Langfang while both have systematic discrepancy in delineating the meridional mean winds. It should be noted that both models represent climatology

but we are comparing with observations from a single season. The agreement might be improved if observations from additional summers were included in the comparisons. On another aspect, the HWM models might be improved by including more observations, especially the observed results over the regions never or less included in the models, for example, the observations over China.

5. Results and discussions: tides

This section presents observations of the tides over Langfang observed by MF radar in the summer of 2009. The short-term variations of the diurnal and semidiurnal tides in the zonal and meridional directions are shown and the mechanisms are discussed briefly. Additionally, the summer-averaged amplitudes and phases for the diurnal and semidiurnal tides, obtained from the summer-averaged 24 hourly-mean zonal and meridional winds by the method described in Section 2, are presented and compared with GSWM-02 and the recent GSWM-09 models.

5.1. Short-term variation of the tides

Fig. 5 gives the temporal and height variations of the semi-diurnal and diurnal tidal amplitudes. Significant short-term semi-diurnal and diurnal tidal variability is observed in both the zonal and meridional wind components over Langfang. The amplitudes in Fig. 5 of zonal semi-diurnal and diurnal tide vary from 2 to 40 m/s; the meridional amplitudes vary over a similar range. The temporal variations in both the zonal and meridional tides show general similarity among different heights. These variations seem regular and are characterized by periods of several days or longer. Lomb–Scargle spectral analysis is applied to the time series of the diurnal and semi-diurnal tidal amplitudes. The method is similar to the spectral analysis of the daily mean winds.

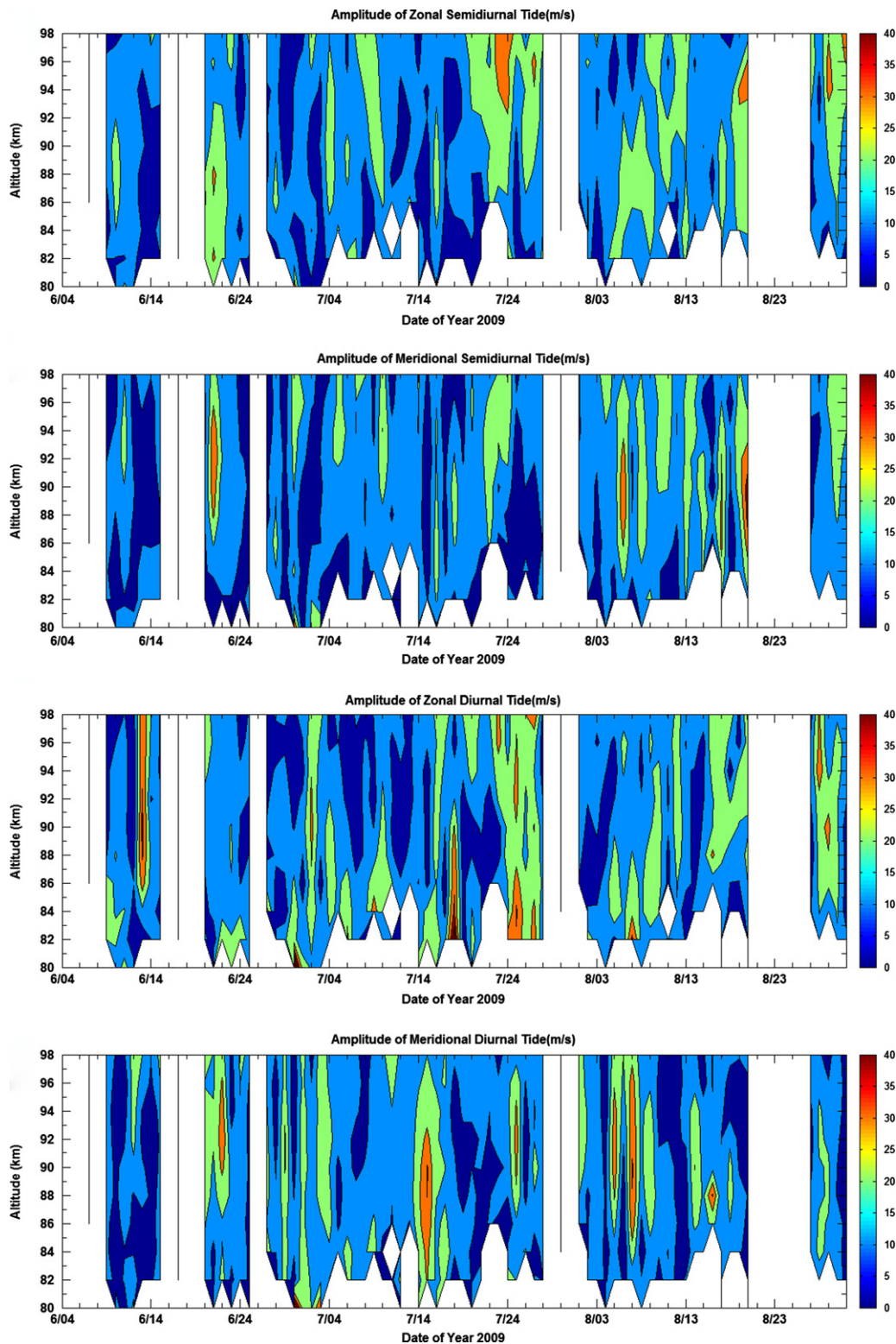


Fig. 5. Temporal variations of the daily semidiurnal and diurnal tidal amplitudes in the zonal and meridional wind components at heights from 80 km to 98 km. (Contour intervals are 10 m/s.)

Fig. 6 shows the spectrum results of the diurnal and semidiurnal tidal amplitudes in the zonal wind components at the height of 90 km. For the diurnal tidal amplitude, the wave spectrum shows that the prominent frequencies are about 0.08 cycles/day and 0.48 cycles/day, denoting the 12.5-day and 2.1-day oscillations, respectively. The frequency 0.08 cycles/day is observed peaked around the date of 17 July with the confidence

of about 82%. The frequency 0.48 cycles/day is found around 5 July with confidence larger than 50%. In addition, the frequencies of 0.13, 0.36, 0.44 cycles/day are present, which denote 7.7-day, 2.8-day and 2.3-day oscillations, respectively. The wave spectrum of the semidiurnal tidal amplitude is dominated by the frequencies of 0.065 cycles/day (i.e., period of 15.4-day) and 0.393 cycles/day (i.e., period of 2.5-day). The frequencies of 0.18,

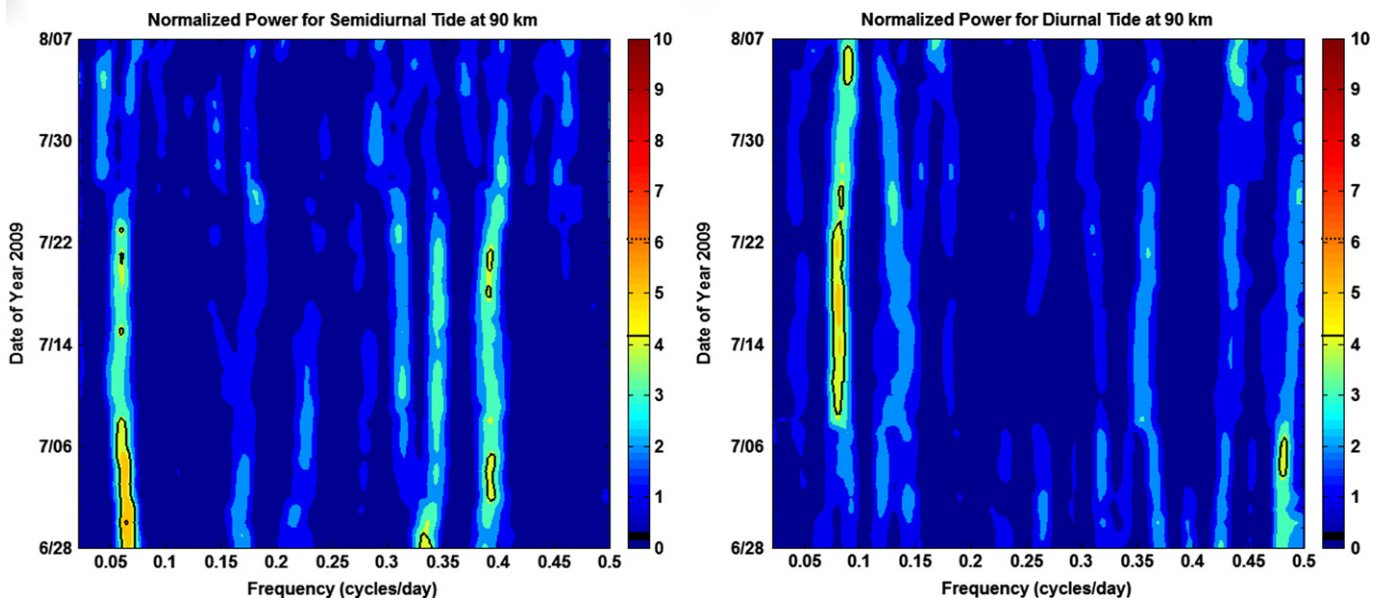


Fig. 6. As Fig. 3, but for the semidiurnal and diurnal tidal amplitudes in the zonal wind components at the height of 90 km.

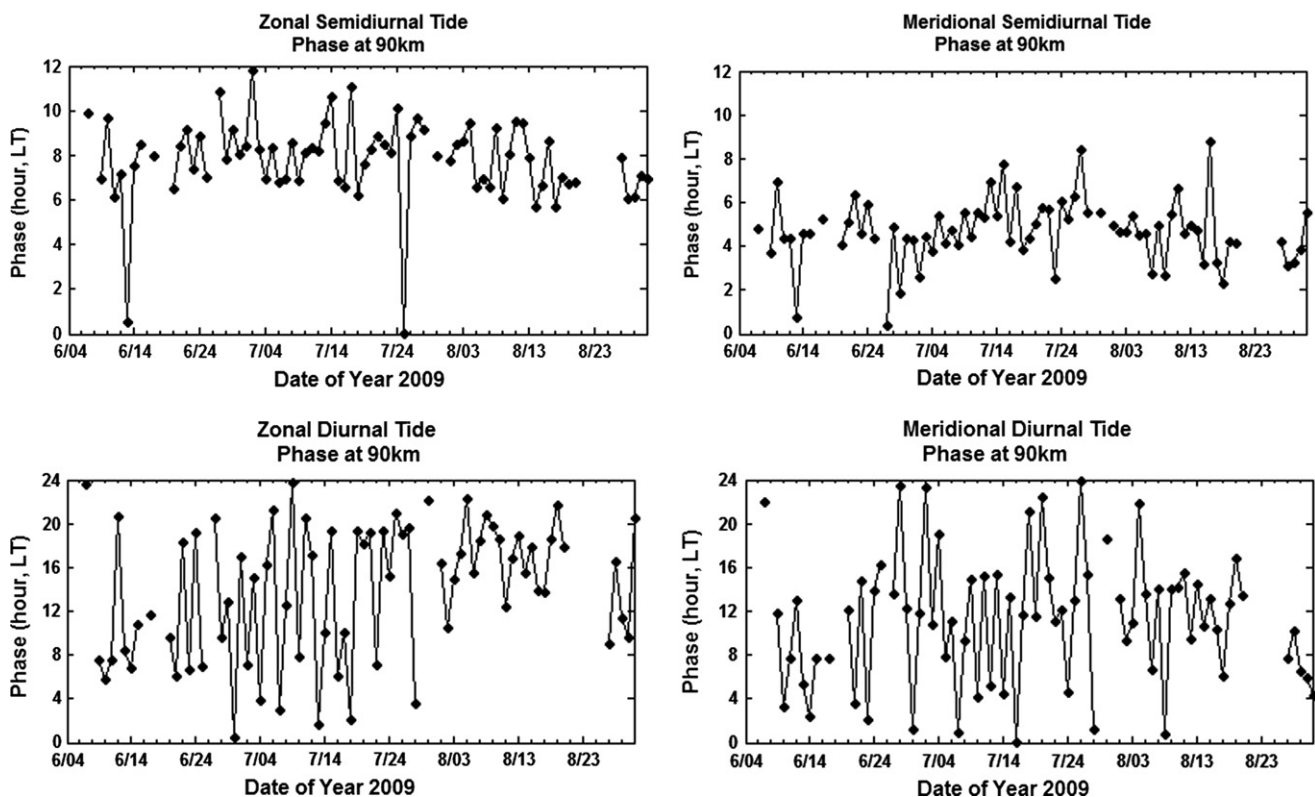


Fig. 7. Phases of the zonal and meridional components of the semidiurnal and diurnal tides at 90 km from June 4 to August 31, 2009.

0.23, 0.35 cycles/day, denoting the 5.6-day, 4.4-day, and 2.9-day oscillations, respectively, are also visible. These spectral results indicate the modulation of tides on time scales on the order of planetary waves, which are consistent with previous results by the frequency analyses of ground-based observations from single or multiple sites (from quasi-two-day to quasi-stationary) (e.g., Nakamura et al., 1997; Kamalabadi et al., 1997; Pancheva, 2000; Pancheva and Mitchell, 2004; She et al., 2004; Nozawa et al., 2006).

To illustrate the tidal phase variability, Fig. 7 presents the phase variations of the diurnal and semidiurnal for the zonal and meridional components at 90 km. The phases for both the zonal and meridional semidiurnal tides in summer show moderate day-to-day variability. This indicates that the phases of the semidiurnal tide do not remain constant over the whole summer, but show a tendency to fluctuate around well-defined mean phases although amplitudes are substantially variable (Fig. 5). The phase of the meridional semidiurnal tide is around 5 h in local time; it

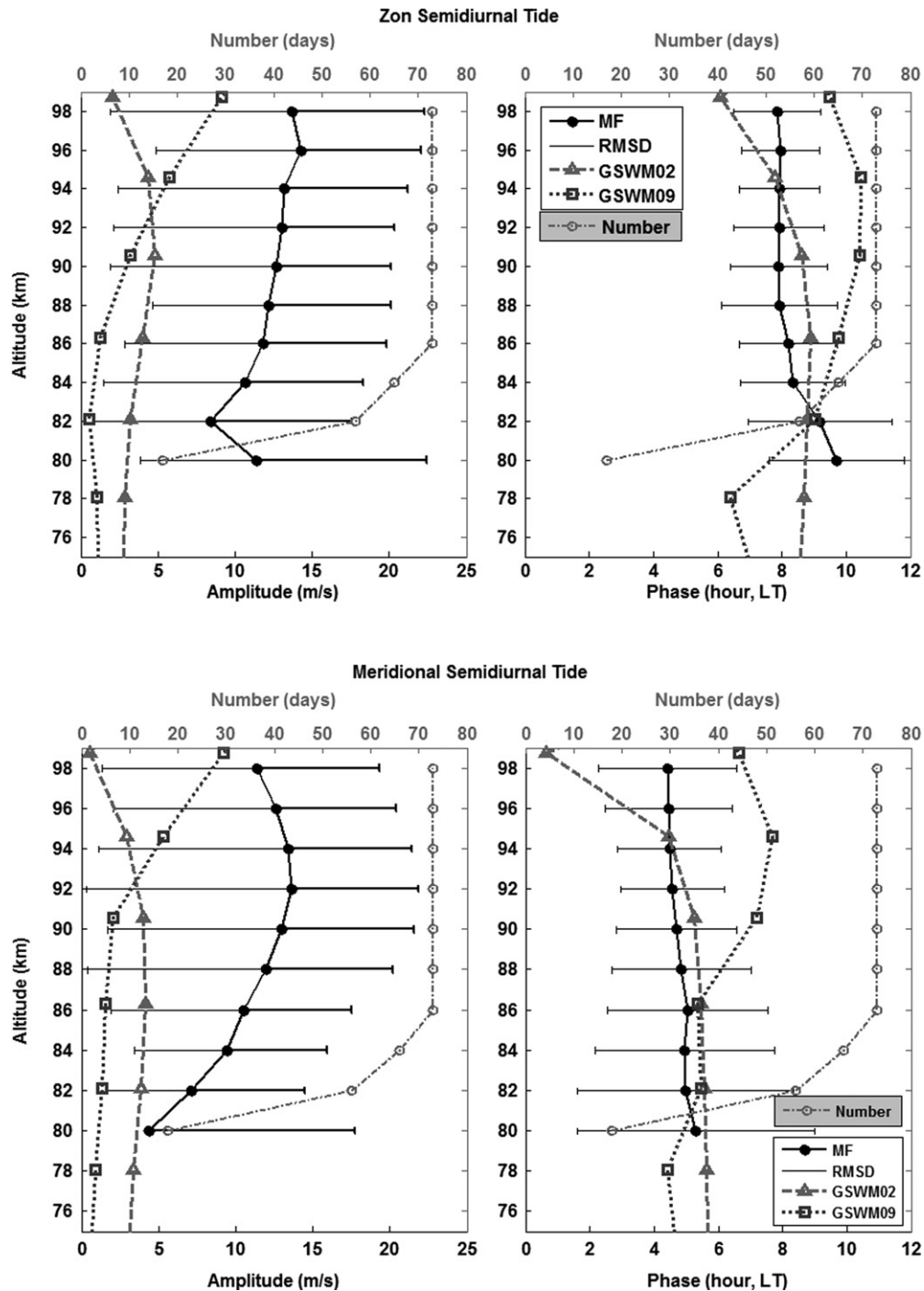


Fig. 8. Summer-averaged amplitudes and phases of the zonal and meridional components of the semidiurnal tides. The solid lines with filled circles denote the results of MF radar, the dashed lines with upward-pointing triangle and dotted lines with square indicate the GSWM-02 and GSWM-09 model results, respectively. The solid horizontal bars denote the RMSD from the daily semidiurnal tides to the summer averages. (It should be noted that for the amplitudes the left end points of the horizontal bars indicate the minima of the daily tidal amplitude while the right sides shown in thicker lines give the RMSD.) The Dash-dot lines with circles give the number of days with observations.

leads that of zonal wind by about 3 h, i.e., ~ 90 degree, consistent with the polarization relations of upward and westward propagating waves. For the diurnal tide, the phases for both the zonal and meridional components of the diurnal tide show fairly large day-to-day variability. The observations made at Langfang often show considerable changes in both amplitude and phase of the diurnal tide from one day to the next. High variability is prevalent at mid-latitudes. For example, observations at (43°N , 81°W) (Thayaparan et al., 1995) also showed high day-to-day variability of the diurnal tide; the semidiurnal tide, by comparison, exhibited relatively more constant phase, although amplitudes could be variable.

These features of substantial short-term variability of the tidal amplitudes and phases could be caused by the interaction of the tides with planetary waves (Hagan and Roble, 2001; Mayr et al., 2005a, 2005b; Ward et al., 2005) or with gravity waves through changes in the mean winds (Fritts and Vincent, 1987; Nakamura et al., 1997) or by a combination of both. As shown in Figs. 5–7, oscillations of tidal amplitudes and phases with periods of several days or longer are present during all the summer months. Comparing the spectra of tides for the zonal mean wind component in Fig. 6 with the spectrum of the zonal daily mean wind in Fig. 3, it is showed that a large part of the tidal variability has the same

periodicity as the planetary waves. The peaks with about 2-day periods in the zonal diurnal and semidiurnal tidal spectra may be coherent with the quasi-2-day planetary waves in Fig. 3; the peaks with about 12.5-day periods and 15.4-day periods may be coherent with the quasi-16-day planetary waves; the peaks with 3–8 days periods can also be found in the spectra of the daily mean winds. These coherent results indicate that the variability of the tides is related with the activities of planetary waves. Based on the simulations with NCAR thermosphere–ionosphere–mesosphere–electrodynamics general circulation model (TIME-GCM) by Liu et al. (2007) and Chang et al. (2011), we know that most probable reason for the large tidal variability is the interaction between the transient planetary wave and tides. Thus, we could attribute the observed apparent changes of tidal amplitudes and phases from one day to the next over Langfang to the contributions of planetary waves, i.e., the interactions of tidal and planetary waves.

5.2. Summer-averaged tides

Figs. 8 and 9 display the summer-averaged amplitude and phase profiles over Langfang as functions of height of the semidiurnal and diurnal tides, respectively, together with the summer-averaged results of GSWM-02 and GSWM-09.

Fig. 8 shows that the amplitudes of the zonal and meridional semidiurnal tides are comparable to each other. In general the amplitudes are in the range of 10–15 m/s. The zonal amplitude shows a modest increase with height above 82 km, while the meridional amplitude increases in the height range of 80–92 km, reaches a maximum value ~ 14 m/s at 92 km and then decreases above. The RMSD, which indicate the day-to-day variability of the semidiurnal amplitudes, are in the range of 6–9 m/s above 82 km; they do not vary much with the height.

The phases of the zonal and meridional components of the semidiurnal tide indicate upward propagation, with the phase downwards (as inferred by the negative phase gradients, i.e., earlier phases at upper heights). This indicates that this 12-hour component is excited below the MLT region. The zonal phase varies from ~ 7.5 h at 98 km to ~ 10 h at 80 km; the most dominant phase is about 8 h in local time. The meridional phase is in the range of 4–5.5 h; the most dominant phase is about 5 h, leading the zonal direction by ~ 3 h. This suggests that the directions of the tidal winds over Langfang rotate clockwise as expected for the northern hemisphere, and the meridional component leads the zonal by approximately 90-degree (also shown in Fig. 7). The phase profile of the zonal semidiurnal tide in Fig. 8 is quite linear in the 84–98 km and 80–84 km height ranges with different slopes. For the meridional semidiurnal component, a linear slope is observed. Above 84 km the zonal downward phase velocity is about 20 km/h and the vertical wavelength is 240 km. Below 84 km the vertical wavelength is about 37 km, while the vertical wavelength of the meridional semidiurnal tide is estimated to be about 144 km. This long vertical wavelength in summer months agrees with previous observations and is most likely due to the dominance of (2, 2) and (2, 3) tidal (Hough) modes (Yuan et al., 2008). The RMSD of the phases are always within two hours for the zonal semidiurnal tide and increase to three hours for meridional tide above 82 km.

The amplitude of the diurnal tide (Fig. 9) is smaller than that of the semidiurnal tide (Fig. 8). The amplitudes of both zonal and meridional diurnal tides are always in the range of 5–10 m/s compared to the 10–15 m/s semidiurnal tide amplitudes. This agrees with most of earlier observations. For example, She et al. (2004) observed much larger semidiurnal zonal wind tides than diurnal tides above 85 km by sodium lidar at Fort Collins (41°N, 105°W) and Manson et al. (1989) characterized the behavior of the diurnal tide at middle latitudes (40–55°) as having smaller amplitudes than the semidiurnal tide. However, some exceptions have also been seen

at 40°N. For example, Franke and Thorsen (1993) showed that the diurnal amplitudes measured by MF radar exceed the semidiurnal amplitudes by a significant amount in March and April below 90 km at Urbana (40°N, 88°W). Manson et al. (2003) also found larger diurnal than semidiurnal amplitudes over Platteville (40°N, 105°W). Since the latitudes of these observations are all the same, the differences may be related to the different longitudes or years or seasons, suggesting the needs for simultaneous and long-continuous measurements at multiple stations.

From Fig. 9, large zonal–meridional differences are found in the height variation of the diurnal amplitudes. For the zonal diurnal tide, the amplitude shows an approximately linear decay from ~ 14 m/s at 82 km to 2 m/s at 88 km and then a linear increase with height above 88 km, reaching ~ 11 m/s at 98 km. The small amplitude at 88 km may be due to the fact that the phases of the diurnal tides change by a large amount from one day to the next (as shown in Fig. 7), leading to cancelation when calculating the summer-averaged hourly-mean zonal winds. On the other hand, the amplitude of the meridional diurnal tide is found to increase moderately with increasing height. At 98 km, the amplitude of the meridional diurnal tide is 11 m/s. The RMSD are in the range of ~ 10 –17 m/s for zonal diurnal amplitudes and range of ~ 8 –13 m/s for meridional diurnal amplitudes above 82 km. At all levels they are larger than those of the semidiurnal amplitudes.

The phases of the diurnal tides are generally less organized than the semidiurnal tides. Their RMSD on the seasonal averages are larger than those of the semidiurnal phases. These, combined with the larger RMSD of the diurnal amplitudes, demonstrate that the day-to-day diurnal tides in summer 2009 are more irregular than semidiurnal tides. In general, downward phase propagation is observed. The vertical wavelength of the zonal diurnal tide above 90 km is about 55 km while that of the meridional diurnal tide above 86 km is about 144 km. Below 86 km, positive phase gradients are observed, which indicate the evanescent nature or the mixture of evanescent and propagating, suggesting in-situ forcing or mode superposition occurring at these heights.

When tidal observations and GSWM-02 and GSWM-09 model results are compared, the agreements in diurnal and semidiurnal phases are generally reasonable while the discrepancies in semidiurnal and diurnal amplitudes are not negligible. Both the GSWM-02 and GSWM-09 underestimate the semidiurnal amplitudes and overestimate the diurnal amplitudes in both zonal and meridional winds. HRDI/UARS winds measurements at 96 km altitude in year 1993–1994 also revealed that GSWM-02 has larger 24-hour tidal amplitudes and smaller 12-hour amplitudes (Manson et al., 2004b).

Fig. 8 shows that GSWM-09 is better than GSWM-02 in simulating the amplitude of the semidiurnal tide above 92 km while below 92 km GSWM-09 departs more from the observation than GSWM-02 by about 2–3 m/s. The semidiurnal phase of GSWM-02 fares a little better than GSWM-09 when compared with the observations. For diurnal comparison in Fig. 9, GSWM-02 and GSWM-09 yield quite similar phase variations, showing propagating nature while data show the evanescent nature below 86 km. Models have shorter vertical wavelengths than the observations. Both the GSWM-02 and GSWM-09 provide an increasingly reasonable estimate of the diurnal tidal characteristics in the MLT region. These two models overestimate the diurnal amplitude while GSWM-09 fares much better. An inspection shows that the GSWM-09 diurnal amplitude typically is a factor of two bigger than the observation and a factor of two smaller than that of GSWM-02, which is especially true for the meridional wind.

Therefore, we can conclude that the prediction of the 2009 summer-averaged diurnal tide over Langfang by GSWM-09 is better than that from GSWM-02 but not the semidiurnal tide. This may be attributed to the fact that no additional data were

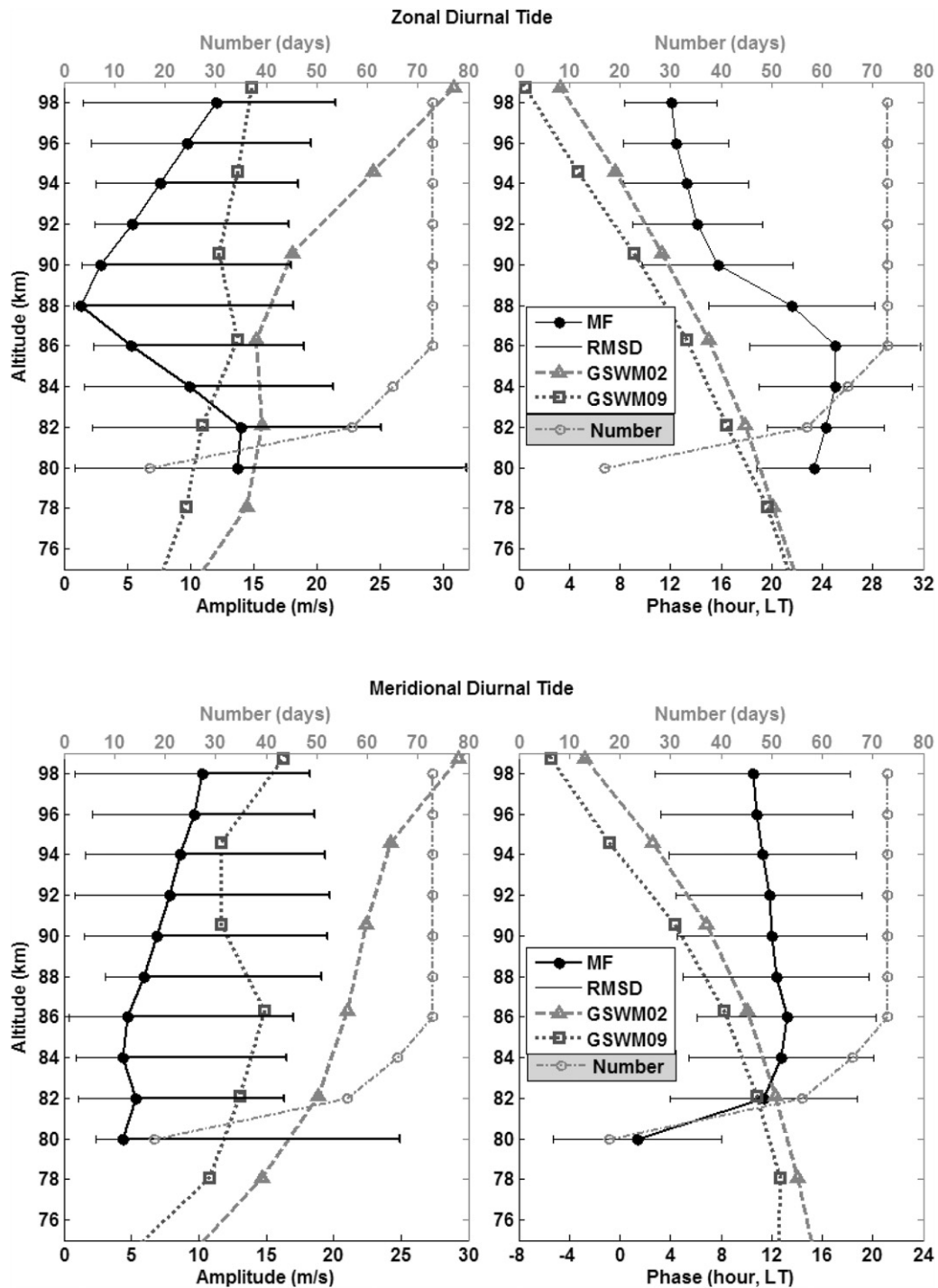


Fig. 9. As Fig. 8, but for diurnal tides.

used in GSWM-09 and so the simulation may miss significant global sources with semidiurnal periods; on the other hand the diurnal tide was adjusted to new data (Zhang et al., 2010a, 2010b).

6. Conclusions

This paper has featured the short-term variability and summer-averages of mean winds and tidal oscillations in the MLT with the newly installed MF radar at Langfang (39.4°N, 116.7°E) during the summer months, 2009. These features are compared with data from other ground-based stations, especially

at ~40°N and with the HWM and GSWM models. Based on the observations and analysis, we have concluded as follows:

- (1) Both the zonal and meridional daily mean winds between 80 km and 98 km over Langfang show considerable day-to-day variability, which are characterized by a superposition of fluctuations on different planetary time scales. The winds could fluctuate from negative tens of meters per second to positive tens of meters per second during the summer days. Their Lomb–Scargle spectral analysis reveals that the quasi-2-day and quasi-16-day planetary waves are active in the MLT region.

- (2) The 2009 summer-averaged zonal wind over Langfang varies almost monotonically from -30 m/s at 80 km to 22 m/s at 98 km with the RMSD about 10 m/s. The wind is westward below 82 km, and eastward above 88 km with the transition altitude at about 85 km. In meridional direction, the summer-averaged wind is dominated by the southward wind. Through most of the range the wind decreases with height. The meridional wind is in the range of -8 m/s to 3 m/s with its RMSD about 10 m/s.
- (3) The comparisons between the summer-averaged winds and the HWM model winds show that HWM-07 overestimates the eastward wind above 84 km by 10–20 m/s, underestimates the westward wind below 84 km by 10 m/s, and overestimates the southward wind by 2–7 m/s. HWM-93 shows almost the same eastward wind above 84 km and underestimates the meridional mean wind by 1–6 m/s. These results suggest that HWM-93 is better than HWM-07 in delineating the 2009-summer averaged zonal wind over Langfang while both have systematic discrepancy in delineating the meridional mean winds.
- (4) Observations made at Langfang during 2009 summer show large changes in both amplitude and phase of the zonal and meridional diurnal tide from one day to the next, and by comparison, the semidiurnal tides fluctuate around well-defined mean phases although amplitudes are variable. The amplitudes of zonal and meridional semidiurnal and diurnal tide vary from 2 to 40 m/s during the summer days with time scales on the order of planetary waves, which are characterized by similar temporal variation among different heights. Lomb–Scargle spectral analysis on the diurnal and semidiurnal tidal amplitudes reveals that a large part of the tidal variability has similar periodicity as the planetary waves. We may attribute these large day-to-day variations of the tides to the contribution of planetary waves.
- (5) Both the 2009 summer-averaged zonal and meridional amplitudes of semidiurnal tides (10–15 m/s) are generally larger than the diurnal tides (~ 5 –10 m/s) over Langfang. The phase of semidiurnal tide propagates downward, indicating this component is excited below the MLT region. For the diurnal tide, downward phase propagation is observed above 86 km whereas positive phase propagation is found below 86 km. This indicates that the tide is evanescent or a mixture of evanescent and propagating. The RMSD of diurnal phases with respect to the seasonal averages are larger than those of the semidiurnal phases. This, combined with the larger RMSD of the diurnal amplitudes, demonstrates that the day-to-day diurnal tides in summer 2009 are more irregular than semidiurnal tides.
- (6) The comparisons between the 2009 summer-averaged tides and the GSWM models show that both GSWM-02 and GSWM-09 underestimate the semidiurnal amplitudes and overestimate the diurnal amplitudes in zonal and meridional wind components; the phases are in somewhat reasonable agreement for the zonal and meridional diurnal tides but not for the semidiurnal tides. GSWM-09 shows evanescent phase propagation for zonal and meridional semidiurnal tides, while the data show downward phase propagation. Additional inspection suggests that the prediction of the 2009 summer-averaged diurnal tide over Langfang by GSWM-09 is better than that from GSWM-02 but not the semidiurnal tide.

The Langfang, China, site has co-located MF and meteor radar and sodium (Na) lidar for simultaneous measurements of horizontal winds in the MLT region. Our future work is to further study the characteristics of tides, planetary wave, and gravity wave activity by using the co-located simultaneous and

continuous data. The measurements will also be combined with data at other mid-latitude stations and satellite observations.

Acknowledgments

This work was supported by the National Natural Science Foundation of China under Grant nos. 41104099 and 40774087. The authors thank Xiaoli Zhang (University of Colorado) for help with the GSWM-09 model.

References

- Andrioli, V.F., Clemesha, B.R., Batista, P.P., Schuch, N.J., 2009. Atmospheric tides and mean winds in the meteor region over Santa Maria (29.7°S, 53.8°W). *Journal of Atmospheric and Solar-Terrestrial Physics* 71, 1864–1876.
- Briggs, B.H., 1984. The analysis of spaced sensor records by correlation techniques. MAP Handbook, vol. 13. SCOSTEP Secretariat, University of Illinois, Urbana, Illinois, pp. 166–186.
- Buriti, R.A., Hocking, W.K., Batista, P.P., Medeiros, A.F., Clemesha, B.R., 2008. Observations of equatorial mesospheric winds over Cariri (7.4°S) by a meteor radar and comparison with existing models. *Annals of Geophysics* 26, 485–497.
- Chang, L.C., Palo, S.E., Liu, H.-L., 2011. Short-term variability in the migrating diurnal tide caused by interactions with the quasi 2 day wave. *Journal of Geophysical Research* 116, D12112, <http://dx.doi.org/10.1029/2010JD014996>.
- Drob, D.P., Emmert, J.T., Crowley, G., Picone, J.M., Shepherd, G.G., Skinner, W., Hays, P., Niciejewski, R.J., Larsen, M., She, C.Y., Meriwether, J.W., Hernandez, G., Jarvis, M.J., Sipler, D.P., Tepley, C.A., O'Brien, M.S., Bowman, J.R., Wu, Q., Murayama, Y., Kawamura, S., Reid, I.M., Vincent, R.A., 2008. An empirical model of the Earth's horizontal wind fields: HWM07. *Journal of Geophysical Research* 113, A12304 <http://dx.doi.org/10.1029/2008JA013668>.
- Emmert, J.T., Drob, D.P., Shepherd, G.G., Hernandez, G., Jarvis, M.J., Meriwether, J.W., Niciejewski, R.J., Sipler, D.P., Tepley, C.A., 2008. DWM07 global empirical model of upper thermospheric storm-induced disturbance winds. *Journal of Geophysical Research* 113, A11319, <http://dx.doi.org/10.1029/2008JA013541>.
- Forbes, J.M., Roble, R.G., Fesen, C.G., 1993. Acceleration, heating and compositional mixing of the thermosphere due to upward propagating tides. *Journal of Geophysical Research* 98, 311–321.
- Forbes, J.M., Zhang, X., Talaat, E.R., Ward, W., 2003. Nonmigrating diurnal tides in the thermosphere. *Journal of Geophysical Research* 108 (A1), 1033, <http://dx.doi.org/10.1029/2002JA009262>.
- Franke, S.J., Thorsen, D., 1993. Mean winds and tides in the upper middle atmosphere at Urbana (40°N, 88°W) during 1991–1992. *Journal of Geophysical Research* 98 (D10), 18,607–18,615, <http://dx.doi.org/10.1029/93JD01840>.
- Friedman, J.S., Zhang, X., Chu, X., Forbes, J.M., 2009. Longitude variations of the solar semidiurnal tides in the mesosphere and lower thermosphere at low latitudes observed from ground and space. *Journal of Geophysical Research* 114, D11114, <http://dx.doi.org/10.1029/2009JD011763>.
- Fritts, D.C., Vincent, R.A., 1987. Mesospheric momentum flux studies at Adelaide, Australia: observations and gravity wave-tidal interaction model. *Journal of Atmospheric Science* 44, 605–619.
- Groves, G.V., Forbes, J.M., 1985. Mean zonal and meridional accelerations and mean heating induced by solar tides for equinox and solstice conditions. *Planetary and Space Science* 33, 283–293.
- Hagan, M.E., Roble, R.G., 2001. Modeling diurnal tidal variability with the national center for atmospheric research thermosphere-mesosphere-electrodynamics general circulation model. *Journal of Geophysical Research* 106, 24869–24882.
- Hagan, M.E., Forbes, J.M., 2002. Migrating and nonmigrating diurnal tides in the middle and upper atmosphere excited by tropospheric latent heat release. *Journal of Geophysical Research* 107 (D24), 4754, <http://dx.doi.org/10.1029/2001JD001236>.
- Hagan, M.E., Forbes, J.M., 2003. Migrating and nonmigrating semidiurnal tides in the upper atmosphere excited by tropospheric latent heat release. *Journal of Geophysical Research* 108 (A2), 1062, <http://dx.doi.org/10.1029/2002JA009466>.
- Hedin, A.E., Spencer, N.W., Killeen, T.L., 1988. Empirical global model of upper thermosphere winds based on atmosphere and dynamics explorer satellite data. *Journal of Geophysical Research* 93 (A9), 9959–9978, <http://dx.doi.org/10.1029/JA093iA09p09959>.
- Hedin, A.E., et al., 1991. Revised global model of thermosphere winds using satellite and ground-based observations. *Journal of Geophysical Research* 96 (A5), 7657–7688, <http://dx.doi.org/10.1029/91JA00251>.
- Hedin, A.E., Fleming, E.L., Manson, A.H., Schmidlin, F.J., Avery, S.K., Clark, R.R., Franke, S.J., Fraser, G.J., Tsuda, T., Vial, F., Vincent, R.A., 1996. Empirical wind model for the upper middle and lower atmosphere. *Journal of Atmospheric and Terrestrial Physics* 58, 1421–1447.
- Iimura, H., Fritts, D.C., Tsutsumi, M., Nakamura, T., Hoffmann, P., Singer, W., 2011. Long-term observations of the wind field in the Antarctic and Arctic mesosphere and lower-thermosphere at conjugate latitudes. *Journal of Geophysical Research* 116, D20112, <http://dx.doi.org/10.1029/2011JD016003>.

- Jiang, G.Y., Xu, J.Y., Shi, J.K., Yang, G.T., Wang, X., Yan, C.X., 2010. The first observation of the atmospheric tides in the mesosphere and lower thermosphere over Hainan, China. *Chinese Science Bulletin* 55, 1059–1066, <http://dx.doi.org/10.1007/s11434-010-0084-8>.
- Kamalabadi, F., Forbes, J.M., Makarov, N.M., Portnyagin, Y.I., 1997. Evidence for nonlinear coupling of planetary waves and tides in the Antarctic mesopause. *Journal of Geophysical Research* 102, 4437–4446.
- Kishore, P., Namboothiri, S.P., Igarashi, K., Murayama, Y., Watkins, B.J., 2002. MF radar observations of mean winds and tides over Poker Flat, Alaska (65.1°N, 147.5°W). *Annals of Geophysics* 20, 679–690.
- Liu, H.L., Li, T., She, C.-Y., Oberheide, J., Wu, Q., Hagan, M.E., Xu, J., Roble, R.G., Mlynczak, M.G., Russell III, J.M., 2007. Comparative study of short-term diurnal tidal variability. *Journal of Geophysical Research* 112, D18108, <http://dx.doi.org/10.1029/2007JD008542>.
- Lu, X., Liu, A.Z., Oberheide, J., Wu, Q., Li, T., Li, Z., Swenson, G.R., Franke, S.J., 2011. Seasonal variability of the diurnal tide in the mesosphere and lower thermosphere over Maui, Hawaii (20.7°N, 156.3°W). *Journal of Geophysical Research* 116, D17103, <http://dx.doi.org/10.1029/2011JD015599>.
- Manson, A.H., Meek, C.E., Teitelbaum, H., Vial, F., Schindler, R., Kürschner, D., Smith, M.J., Fraser, G.J., Clark, R.R., 1989. Climatologies of semi-diurnal and diurnal tides in the middle atmosphere (70–110 km) at middle latitudes (40–55°). *Journal of Atmospheric and Terrestrial Physics* 51, 579–593.
- Manson, A.H., Meek, C.E., Hall, G.E., 1998. Correlations of gravity waves and tides in the mesosphere over Saskatoon. *Journal of Atmospheric and Solar-Terrestrial Physics* 60, 1089–1107.
- Manson, A.H., Meek, C., Hagan, M., Koshyk, J., Franke, S., Fritts, D., Hall, C., Hocking, W., Igarashi, K., Macdougall, J., Riggan, D., Vincent, R., 2002. Seasonal variations of the semi-diurnal and diurnal tides in the MLT: multi-year MF radar observations from 2–70°N, modelled tides (GSWM, CMAM). *Annals of Geophysics* 20, 661–677.
- Manson, A.H., Meek, C.E., Avery, S.K., Thorsen, D., 2003. Ionospheric and dynamical characteristics of the mesosphere-lower thermosphere region over Platteville (40°N, 105°W) and comparisons with the region over Saskatoon (52°N, 107°W). *Journal of Geophysical Research* 108 (D13), 4398, <http://dx.doi.org/10.1029/2002JD002835>.
- Manson, A.H., Meek, C.E., Avery, S.K., Thorsen, D., Hocking, W.K., MacDougall, J.W., Igarashi, K., Namboothiri, S.P., Murayama, Y., 2004a. Longitudinal and latitudinal variations in dynamic characteristics of the MLT (70–95 km): a study involving the CUJO network. *Annals of Geophysics*, 347–365.
- Manson, A.H., Meek, C., Hagan, M., Zhang, X., Luo, Y., 2004b. Global distributions of diurnal and semidiurnal tides: observations from HRDI-UARS of the MLT region and comparisons with GSWM-02 (migrating, nonmigrating components). *Annals of Geophysics* 22, 1529–1548, <http://dx.doi.org/10.5194/angeo-22-1529-2004>.
- Mayr, H.G., Mengel, J.G., Talaat, E.R., Porter, H.S., Chan, K.L., 2005a. Mesospheric non-migrating tides generated with planetary waves: I. Characteristics. *Journal of Atmospheric and Solar-Terrestrial Physics* 67, 959–980.
- Mayr, H.G., Mengel, J.G., Talaat, E.R., Porter, H.S., Chan, K.L., 2005b. Mesospheric non-migrating tides generated with planetary waves: II. Influence of gravity waves. *Journal of Atmospheric and Solar-Terrestrial Physics* 67, 981–991.
- Nakamura, T., Fritts, D.C., Isler, J.R., Tsuda, T., Vincent, R.A., Reid, I.M., 1997. Short-period fluctuations of the diurnal tide observed with low-latitude MF and meteor radars during CADRE: evidence for gravity wave/tidal interactions. *Journal of Geophysical Research* 102, 26225–26238.
- Namboothiri, S.P., Manson, A.H., Meek, C.E., 1993. E region real heights and their implications for MF radar-derived wind and tidal climatologies. *Radio Science* 28, 187–202.
- Nozawa, S., Ogawa, Y., Brekke, A., Tsuda, T., Hall, C.M., Miyaoka, H., Kurihara, J., Abe, T., Fujii, R., 2006. EISCAT observational results during the DELTA campaign. *Earth, Planets and Space* 58, 1183–1191.
- Pancheva, D.V., 2000. Evidence for nonlinear coupling of planetary waves and tides in the lower thermosphere over Bulgaria. *Journal of Atmospheric and Solar-Terrestrial Physics* 62, 115–132.
- Pancheva, D.V., Mitchell, N.J., 2004. Planetary waves and variability of the semidiurnal tide in the mesosphere and lower thermosphere over Esrange (68°N, 21°E) during winter. *Journal of Geophysical Research* 109, A08307, <http://dx.doi.org/10.1029/2004JA010433>.
- Pancheva, D., Mukhtarov, P., Andonov, B., 2009. Global structure, seasonal and interannual variability of the migrating semidiurnal tide seen in the SABER/TIMED temperatures (2002–2007). *Annals of Geophysics* 27, 687–703, <http://dx.doi.org/10.5194/angeo-27-687-2009>.
- Press, W.H., Teukolsky, S.A., Vetterling, W.T., Flannery, B.O. (Eds.), 1992. *Numerical Recipes in FORTRAN*, 2nd Edition Cambridge University Press, Cambridge.
- She, C.Y., Li, T., Collins, R.L., Yuan, T., Williams, B.P., Kawahara, T., Vance, J.D., Acott, P., Krueger, D.A., Liu, H.L., Hagan, M.E., 2004. Tidal perturbations and variability in the mesopause region over Fort Collins, CO (41N, 105W): continuous multi-day temperature and wind lidar observations. *Geophysical Research Letters* 31, L24111, <http://dx.doi.org/10.1029/2004GL021165>.
- Shepherd, G.G., Roble, R.G., Zhang, S.-P., McLandress, C., Wiens, R.H., 1998. Tidal influence on midlatitude airglow: comparison of satellite and ground-based observations with TIME-GCM predictions. *Journal of Geophysical Research* 103 (A7), 14,741–14,751, <http://dx.doi.org/10.1029/98JA00884>.
- Thayaparan, T., Hocking, W.K., MacDougall, J., 1995. Middle atmospheric winds and tides over London, Canada (43°N, 81°W) during 1992–1993. *Radio Science* 30 (4), 1293–1309, <http://dx.doi.org/10.1029/95RS00803>.
- Ward, W.E., Fomichev, V.I., Beagley, S., 2005. Nonmigrating tides in equinox temperature fields from the Extended Canadian Middle Atmosphere Model (CMAM). *Geophysical Research Letters* 32, L03803, <http://dx.doi.org/10.1029/2004GL021466>.
- Xiao, C.Y., Hu, X., Zhang, X.X., Zhang, D.Y., Wu, X.C., Gong, X.Y., Igarashi, K., 2007. Interpretation of the mesospheric and lower thermospheric mean winds observed by MF radar at about 30°N with the 2D-SOCRATES model. *Advances in Space Research* 39 (8), 1267–1277.
- Yi, F., 2001. Short-term variability and temporary structures of tides and mean wind in the polar summer mesosphere. *Journal of Atmospheric and Solar-Terrestrial Physics* 63, 749–757.
- Yuan, T., Schmidt, H., She, C.Y., Krueger, D.A., Reising, S., 2008. Seasonal variations of semidiurnal tidal perturbations in mesopause region temperature and zonal and meridional winds above Fort Collins, Colorado (40.6°N, 105.1°W). *Journal of Geophysical Research* 113, D20103, <http://dx.doi.org/10.1029/2007JD009687>.
- Zhang, S.D., Yi, F., Hu, X., 2004. MF radar observation of mean wind and tides of winter mesopause (80–98 km) region over Wuhan (30°N–114°E). *Journal of Atmospheric and Solar-Terrestrial Physics* 66, 15–25.
- Zhang, X., Forbes, J.M., Hagan, M.E., 2010a. Longitudinal variation of tides in the MLT region: 1. Tides driven by tropospheric net radiative heating. *Journal of Geophysical Research* 115, A06316, <http://dx.doi.org/10.1029/2009JA014897>.
- Zhang, X., Forbes, J.M., Hagan, M.E., 2010b. Longitudinal variation of tides in the MLT region: 2. Relative effects of solar radiative and latent heating. *Journal of Geophysical Research* 115, A06317, <http://dx.doi.org/10.1029/2009JA014898>.